Catal Lett (2008) 123:173–180
DOI 10.1007/s10562-008-9490-9

Enhancing Photocatalytic Activity of Polymorphic Titania Nanoparticles by NMP Solvent-based Ambient Condition Process

Sujaree Kaewgun · Christopher A. Nolph · Burtrand I. Lee

Received: 21 January 2008 / Accepted: 11 April 2008 / Published online: 30 April 2008

Abstract Solvent-based ambient condition sol (SACS) process with *N*-methylpyrrolidone (NMP) as the solvent, is a post-treatment technique utilized to modify polymorphic titania nanoparticles prepared by a water-based ambient condition sol process. All samples were characterized by X-ray diffraction, N_2 physisorption, CHNS analysis, UV–vis absorption spectrophotometry, FT-IR, and TEM and compared to a commercial reference titania product, Degussa P25. Photocatalytic activity, evaluated by the degradation of methyl orange under ultraviolet (UV) and visible light (VL), showed that SACS, with NMP as the solvent, is a powerful treatment to enhance TiO_2 photocatalytic activity by minimizing lattice hydroxyls and doping titania samples with nitrogen.

Keywords Polymorphic titania · Solvothermal · Photocatalytic activity

1 Introduction

One of the most well-known photocatalysts is titanium dioxide or titania (TiO_2), and it is commonly used for industrial applications such as an antibacterial agent, water/air purifier, deodorizer, pigment, semiconductor and, in general, decomposition of organic compounds under UV light irradiation [1–6]. There are three TiO_2 polymorphs: anatase, rutile, and brookite, which have similar chemical properties and band gap energies ($\sim 3.1 \pm 0.1$ eV), but different crystalline structures. Anatase and rutile are tetragonal [3], however brookite is orthorhombic [7]. Anatase TiO_2 has been reported to be more photocatalytically active under UV exposure than rutile [2, 3, 6], but rutile TiO_2 is the most thermodynamically stable phase. Not many studies exist on brookite TiO_2 due to the difficult preparation of single phase brookite TiO_2. A few publications from this group [7–9] reported a water-based ambient condition sol (WACS) for producing predominantly brookite titania. Degussa Aeroxide TiO_2 P25 (P25) [10], consisting of 79% anatase 21% rutile, is an excellent photocatalyst under UV light.

Solvothermal synthesis was reported by Sato et al. [11] to be an excellent technique to synthesize highly crystalline fine particles. Yin et al. [12–14] explained that solvothermal titania samples prepared with ethanol or methanol showed a higher photocatalytic activity than titania samples prepared by hydrothermal reactions. The authors explained this by a higher degree of crystallinity in the solvothermal samples which meant fewer defects and thus a lower recombination rate of electrons and holes. Another study showed that nitrogen-doped titania samples prepared by a homogenous precipitation-solvothermal process in methanol or ethanol solutions possessed superior photocatalytic activity for nitrogen monoxide destruction than those prepared in a completely aqueous solution. Again, the solvothermal technique produced a greater degree of crystallinity in the structure, and yielded a higher specific surface area [15].

Our previous solvothermal titania study [16] utilized a technique developed from barium titanate treatment [17, 18]. The solvothermal post-treatment with sec-butanol as the solvent produced a lower lattice hydroxyl content in polymorphic titania nanoparticles thus enhancing the photocatalytic activity. In this paper, photocatalytic activity of

S. Kaewgun · C. A. Nolph · B. I. Lee (✉)
School of Materials Science and Engineering,
Clemson University, Clemson, SC 29634, USA
e-mail: burt.lee@ces.clemson.edu

titania that was prepared by solvent-based ambient condition sol (SACS) process using *N*-methylpyrrolidone (NMP) is reported. NMP is a nitrogen containing high boiling point (~202 °C) organic solvent. Because of its high boiling point, we will be able to apply high temperature (170 °C) during the solvothermal treatment. Doping titania, especially anatase titania, with nitrogen has been widely reported to improve the photocatalytic activity under visible light irradiation by narrowing the band gap of titania [19, 20]. However, few visible light active polymorphic titania studies using a solvothermal treatment have been done. WACS and SACS with NMP solvent polymorphic titania were investigated by various physical characterization techniques and photocatalytic activities under both ultraviolet (UV) and visible light (VL) irradiation, evaluated by the degradation of methyl orange. They were also compared to a commercial reference, Degussa P25.

2 Experimental

The WACS process, titanium tetrachloride ($TiCl_4$—Reagent grade obtained from Aldrich Chemical) in a 1:2 ratio of water–isopropanol solution with 0.3 M hydrochloric acid under refluxing conditions at 83 °C for 15 h [7–9], was used to prepare polymorphic TiO_2. A post-treatment to the WACS process, called SACS [16–18], was carried out in *N*-methylpyrrolidone (NMP) at 170 °C for 4 h in a sealed Teflon container. WACS samples were calcined in air at 200 °C for 2 h, and the SACS samples were calcined at various temperatures in air for 2 h. The nomenclature to be used throughout this paper, preparation conditions, and % phase composition of titania samples are shown in Table 1.

An X-ray diffractometer was used to determine phase composition and crystallite size of the TiO_2 samples using an XDS 2000, Scintag PAD V with CuK_α radiation at 1.5406 Å, measured with a step size of 0.020° over a range of 20–35° (2θ). The phase composition of titania was calculated from the following equations used by Zhang and Banfield [21]:

$$W_A = \frac{k_A A_A}{k_A A_A + A_R + k_B A_B}, \quad (1)$$

$$W_B = \frac{k_B A_B}{k_A A_A + A_R + k_B A_B}, \quad (2)$$

$$W_R = \frac{A_R}{k_A A_A + A_R + k_B A_B}, \quad (3)$$

where W_A, W_B, and W_R represent the weight fractions of the anatase, brookite, and rutile phases, respectively; k_A is 0.886 and k_B is 2.721 [21]; A_A, A_B, and A_R are the integrated intensities of the anatase (101), brookite (121), and rutile (110) peaks, respectively. For pure brookite, $I^{(121)}_{brookite}/I^{(120)}_{brookite}$ intensity ratio is approximately 0.9 [22, 23]. Therefore, we de-convoluted anatase (101) and brookite (120) overlap peaks by using 0.9 factor. The Scherrer equation (Eq. 4) was applied to calculate titania crystallite size from the full-width half-height of the diffraction peak from the XRD patterns.

$$t = \frac{0.9 \cdot \lambda}{\beta \cdot \cos(\theta)} \quad (4)$$

where, λ is X-ray wavelength, 1.5418 Å for CuK_α, and β is the full-width half-height of the peak of interest: (121) for brookite, (110) for anatase and (101) for rutile [24].

The BET surface area, pore volume, and average pore diameter of the samples were determined by N_2 physisorption at −196 °C using a Micromeritics ASAP 2020

Table 1 Experimental conditions utilized to produce polymorphic titania and % titania phase content

Sample ID	% Content of TiO_2 Phase (wt.%)[a]			Mode of formation	Preparation or post-treated temperature (°C)	Preparation or post-treated time (h)
	An	Br	Ru			
WACS	48	50	2	WACS	83	15
WACS-200	45	53	2	Calcination of WACS	200	2
SACS	42	55	3	SACS of WACS	170	4
SACS-200	44	53	3	Calcination of SACS	200	2
SACS-250	38	60	2		250	2
SACS-300	45	51	4		300	2
SACS-350	34	62	4		350	2
SACS-400	28	65	7		400	2
SACS-500	19	58	23		500	2
P25	79	–	21	Obtained from Degussa	N/A	N/A

An, anatase; Br, brookite; Ru, rutile

[a] Obtained from XRD data by calculating from Eqs. 1 to 3

automated system. A sample amount of 0.3–0.5 g was degassed at 200 °C for 3 h prior to N_2 physisorption. The particle size and morphology of titania samples were investigated by transmission electron microscopy (TEM), obtained from a Hitachi TEM H7600 with an accelerating voltage of 120.0 kV. TEM samples were prepared by dispersing titania powder, 0.01 g, in isopropanol via ultrasonication, transferring the suspension drop-wise to copper TEM sample grids, and allowing isopropanol to evaporate.

The amount of nitrogen was determined using a CHNS analyzer (Perkin–Elmer 2400 series II). Absorbance spectra of titania samples were recorded by UV/Vis spectrophotometer using a GretagMacbeth Color i5 spectrometer across a UV/Vis range of 360–750 nm.

The relative concentrations of lattice hydroxyls and surface hydroxyls to a titania reference peak were calculated from FT-IR spectra based on our previous work [16, 18, 25–27]. The vibrational bands for total water and $^{-}$OH groups were observed by FT-IR, using Thermo-Nicolet Magna model 550 FT-IR spectrometer equipped with a Thermo-Spectra Tech foundation series diamond attenuated total reflection (ATR) accessory. Absorption bands were observed from 4,000 to 525 cm^{-1} with 32 sample scans. FT-IR spectra deconvolution was applied by using "fityk 0.7.4" curve fitting program (the GNU General Public License, version 2, as published by the Free Software Foundation) as shown in Fig. 5b. Previous research on titania in this group [16] has confirmed that the ATR is a valid technique for the semiquantitative analysis of hydroxyls since the results obtained from diffuse reflectance infrared Fourier transform (DRIFT) and ATR techniques were essentially the same. The peak ratios of the absorption bands for hydroxyls to that of titania, following the previous work for barium titanate [25–27] and titania [16], were calculated for a semiquantitative analysis of the hydroxyl content.

The photocatalytic degradation of the methyl orange (MO) by UV and VL irradiation was used to evaluate the photocatalytic activities. The minimal amount of titania to obtain a discernable difference between samples, 0.1 g for UV measurements and 0.2 g for VL irradiation, was added to 100 mL of 20 μM MO solution, and then stirred for 30 min without UV or VL exposure and continuously stirred throughout the reaction procedure. A Spectroline black light lamp (Model BIB-150B operating at 365 nm and 182 W) was used as the UV light source, which was positioned 36 cm above the MO solution. The VL source was a compact fluorescent lamp (Philips energy saver 60 soft white A19, 14 W) with wavelength of 560–612 nm. A portion of the suspension was taken at constant time increments, and titania powders were separated from the solution by vacuum filtration. The quantitative spectral results were monitored by a UNICAM UV/Vis spectrometer (Model: 5625). The methyl orange degradation percent value (D) was calculated by Eq. 5.

$$D = \frac{C_0 - C}{C_0} \times 100\% = \frac{A_0 - A}{A_0} \times 100\% \quad (5)$$

where, C_0 is the initial MO concentration, C is the instantaneous MO concentration, A_0 is the initial 490 nm absorbance peak intensity, and A is the instantaneous 490 nm peak intensity.

3 Results and Discussion

Identification of titania phases, confirmed by comparison to accepted standard peaks from JCPDS [22, 28, 29], were obtained from X-ray diffraction (XRD). XRD patterns of the TiO_2 samples are shown in Fig. 1. The percent of TiO_2 phases contained within each sample, calculated from XRD data, are shown in Table 1. The phase composition of uncalcined (WACS and SACS) and calcined titania samples at 200–350 °C for 2 h (WACS-200, SACS-200, SACS-250, SACS-300, and SACS-350) varied as follows: 50–62% brookite, 34–48% anatase, and less than 5% rutile. Increasing the calcination temperature above 350 °C, a greater portion of rutile was introduced to the structure. Table 2 summarizes the crystallite sizes calculated from the XRD data using the Scherrer equation. The crystallite sizes of brookite and anatase phases for WACS, WACS-200, SACS, and SACS samples calcined at 200–300 °C for

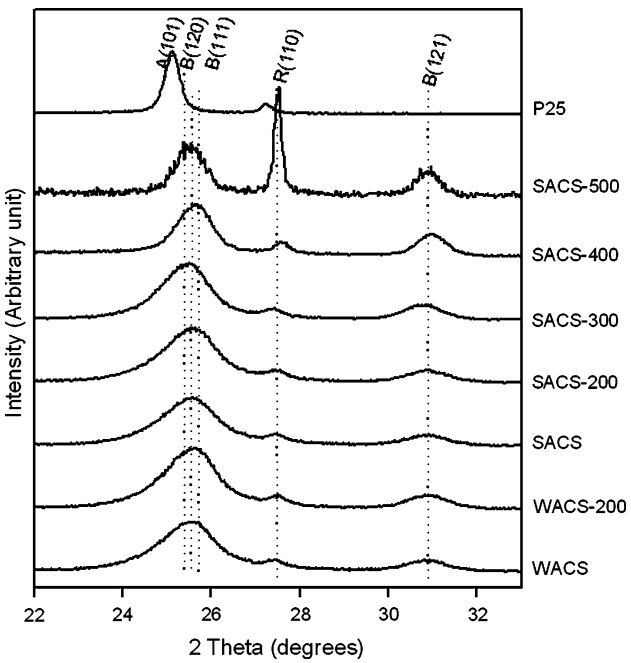

Fig. 1 The XRD pattern of the prepared titania samples and P25. A, anatase; B, brookite; R, rutile

Table 2 The physical properties of prepared titania and the reference P25

Sample ID	Crystallite size (nm)[a]			Average particle size (nm)[b]	BET surface area (m^2/g)[c]	Pore volume (cm^3/g)[c]	Pore size average (Å)[c]
	Anatase	Brookite	Rutile				
WACS	6	8	19	6	163	0.1	25
WACS-200	6	7	18	7	157	0.1	27
SACS	7	8	12	6	133	0.1	24
SACS-200	6	8	11	7	138	0.1	25
SACS-250	5	8	13	N/A	157	0.1	26
SACS-300	6	8	13	9	143	0.1	29
SACS-350	7	10	17	N/A	88	0.1	48
SACS-400	8	10	20	14	68	0.1	60
SACS-500	7	20	71	18	34	0.1	108
P25	21	–	40	40	56	0.2	169

[a] Calculated from XRD data using the Scherrer equation (Eq. 4). Error of measurement = ±5%

[b] Determined by using TEM micrograph

[c] Using N_2 physisorption at 77 K. Error of measurement = ±10%

2 h ranged from 5 to 8 nm which is approximately three times smaller than anatase phase crystallite size of P25. Above 300 °C, the increasing calcination temperature increased the crystallite size of SACS samples.

Table 2 shows the results of BET surface area analysis, pore volume, and average pore diameter of titania samples. The BET surface area of prepared titania samples were three times larger than that of P25 samples. The effect of the calcination temperature of SACS samples on the BET surface area and the nitrogen content in the samples are given in Fig. 2. The BET surface area of uncalcined titania (WACS and SACS) is equivalent to calcined samples at 200 °C for 2 h in air (WACS-200 and SACS-200), respectively, since all samples were pre-treated at 200 °C for 3 h in N_2. SACS and SACS-200 samples have approximately 15–20% smaller surface area than WACS and WACS-200 samples. This is most likely because NMP resided on the titania surface and could not be completely removed during the calcination at temperature below 200 °C for 2 h. The surface area of SACS shows an increasing trend up to 250–300 °C calcination temperatures. Above 300 °C, the surface area decreased with increasing the temperature. The surface area of SACS-250 and SACS-300 are similar to that of WACS samples. All NMP and nitrogen in SACS samples were likely released by calcination at the temperatures above 250 °C. This assessment is supported by CHNS analysis, which shows no nitrogen in SACS-300 and SACS-400. Visible observation of the color of SACS, SACS-200, and SACS-250 is brown, which indicates nitrogen formed or NMP remaining on the surface and in the structure, on the other hand SACS-300, SACS-350, SACS-400, and SACS-500 powders are white. The surface area of SACS samples, calcined at temperatures above 350 °C, rapidly decreased since the titania nanoparticles were sintered during the heat treatment. TEM micrographs are shown in Fig. 3 and Table 2 shows the average particle size of TiO_2 as determined from TEM micrographs. The average particle size of as-prepared titania samples are much smaller than P25. As the calcination temperature is increased, the average particle size of the polymorphic titania slightly increased at temperatures below 300 °C. Above 300 °C, the average particle size increased linearly with increasing temperature by the sintering of nanoparticles during the heat treatment.

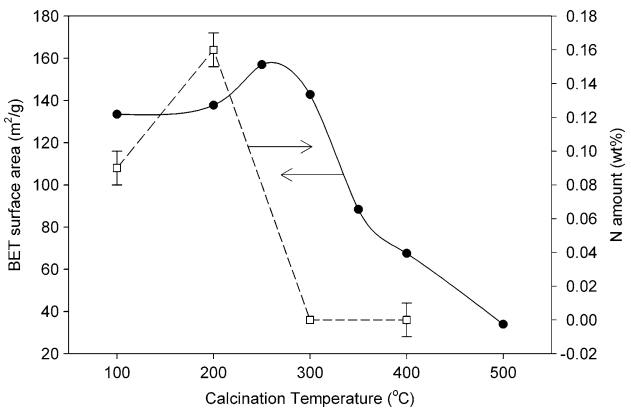

Fig. 2 The effect of calcination temperature for SACS samples on BET surface area and nitrogen content

UV/Vis spectra of titania samples are shown in Fig. 4. SACS samples exhibited visible light active potential by shifts of the absorption shoulders to the visible light region, compared with P25 and WACS-200 in the inset of Fig. 4. The increase in absorbance at wavelengths greater than 550 nm, in increasing order is SACS ≅ SACS-200 ≅ SACS-250 > SACS-300 >> SACS-350 > SACS-400 ≅ WACS-200 > SACS-500 ≅ P25. The more nitrogen

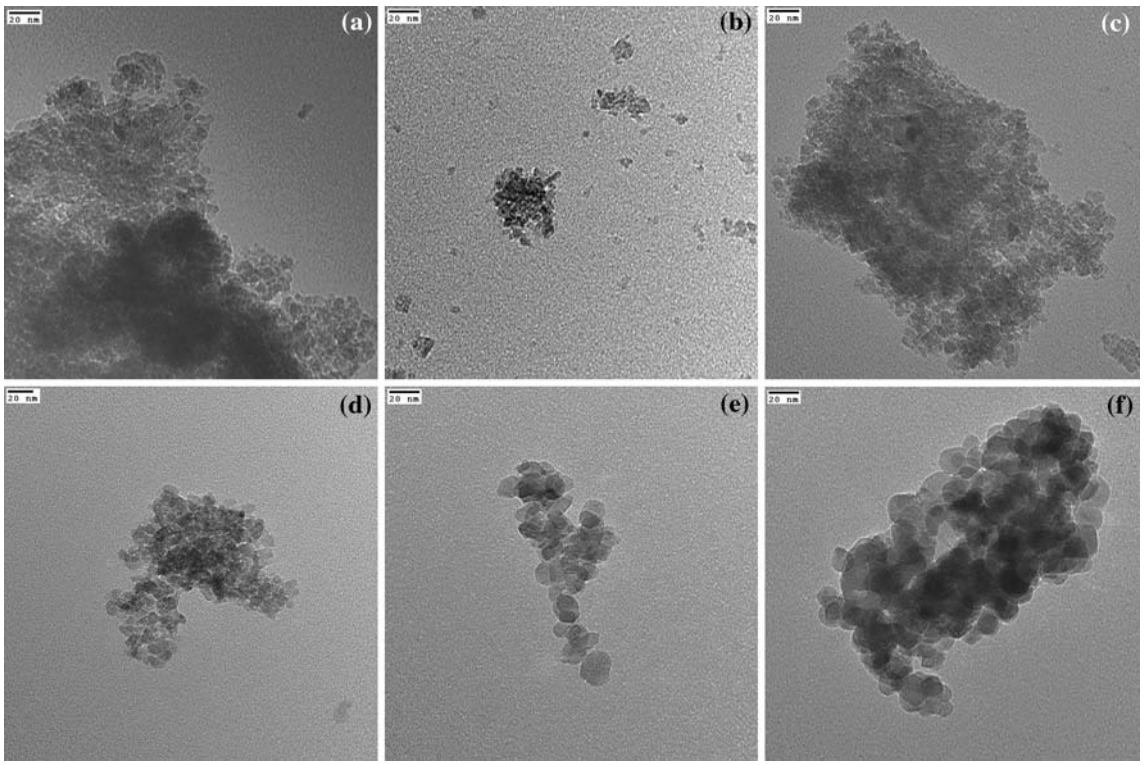

Fig. 3 SEM micrographs of (**a**) WACS-200, (**b**) SACS, (**c**) SACS-200, (**d**) SACS-300, (**e**) SACS-400, and (**f**) SACS-500

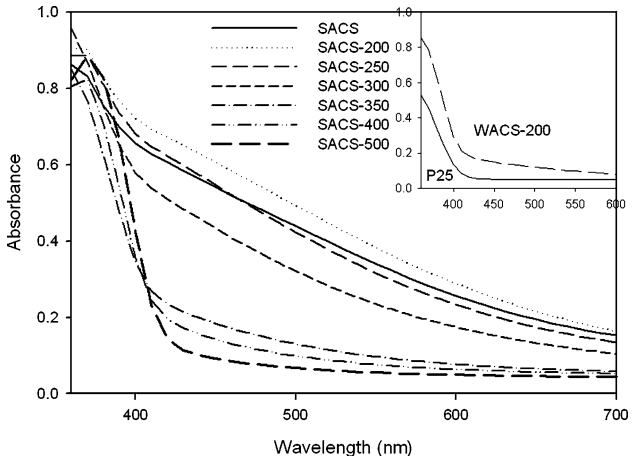

Fig. 4 UV/Vis spectra of as-prepared SACS samples; Inset shows UV/Vis spectra of WACS-200 and P25

found in the samples, given by CHNS analysis, the greater visible light absorption. Because of N atoms in SACS-NMP samples, a narrowing of titania band gap occurs [19, 20, 30–38]. The mechanism that N-doped TiO_2 responds to visible light arises from the formation of a N-induced mid-gap level slightly above the (O-2*p*) valence band edge was determined by Nakamura et al. [35]. The authors concluded that N ions were substituted at oxygen sites in TiO_2 to achieve a narrower titania band gap. In support of the evaluation for nitrogen present in SACS-NMP samples, XPS spectra of SACS-200 revealed a main N 1s peak at 398.3 eV, which indicates the anionic N^- in O–Ti–N linkages [36], and some small peaks from 395.5 to 398 eV which are anionic nitride (N^{3-}) in TiN [39–41].

The obtained FT-IR spectra for SACS and WACS titania samples are given in Fig. 5a. Deconvolution of the spectra, illustrated in Fig. 5b, gave rise to four peaks at 1,625, 2,730, 3,130, and 3,400 cm^{-1}. The $^-$OH stretching vibrations of hydrogen-bonded $^-$OH groups (lattice hydroxyls), and adsorbed molecular water absorption bands (surface hydroxyls) can be found at wavenumbers around 3,400–3,500, and 1,625 cm^{-1}, respectively [16, 42–44]. Analysis of the FT-IR spectra is given in Fig. 5c, containing the calculated relative band intensities for surface and lattice hydroxyls. The peaks fitting result of WACS-200 by fityk 0.7.4 program is shown in the inset of Fig. 5c. In order to compare the amount of hydroxyls given by FT-IR spectra, the band intensities of hydroxyls were normalized with the band intensity of the Ti–O stretching band. The baseline method, as reported in the literature [16, 18, 25–27], was applied to calculate band intensity ratios (A_S/A_T and A_L/A_T) of the absorbance peaks of surface hydroxyls (A_S) at wavenumber 1,625 cm^{-1} and a broad band centered at approximately 3,400 cm^{-1}, the lattice hydroxyls peak (A_L), to the reference peak for titania (A_T), the same wavenumber for all samples at 900 cm^{-1}. The semiquantitative comparison of band intensities indicates that WACS-200,

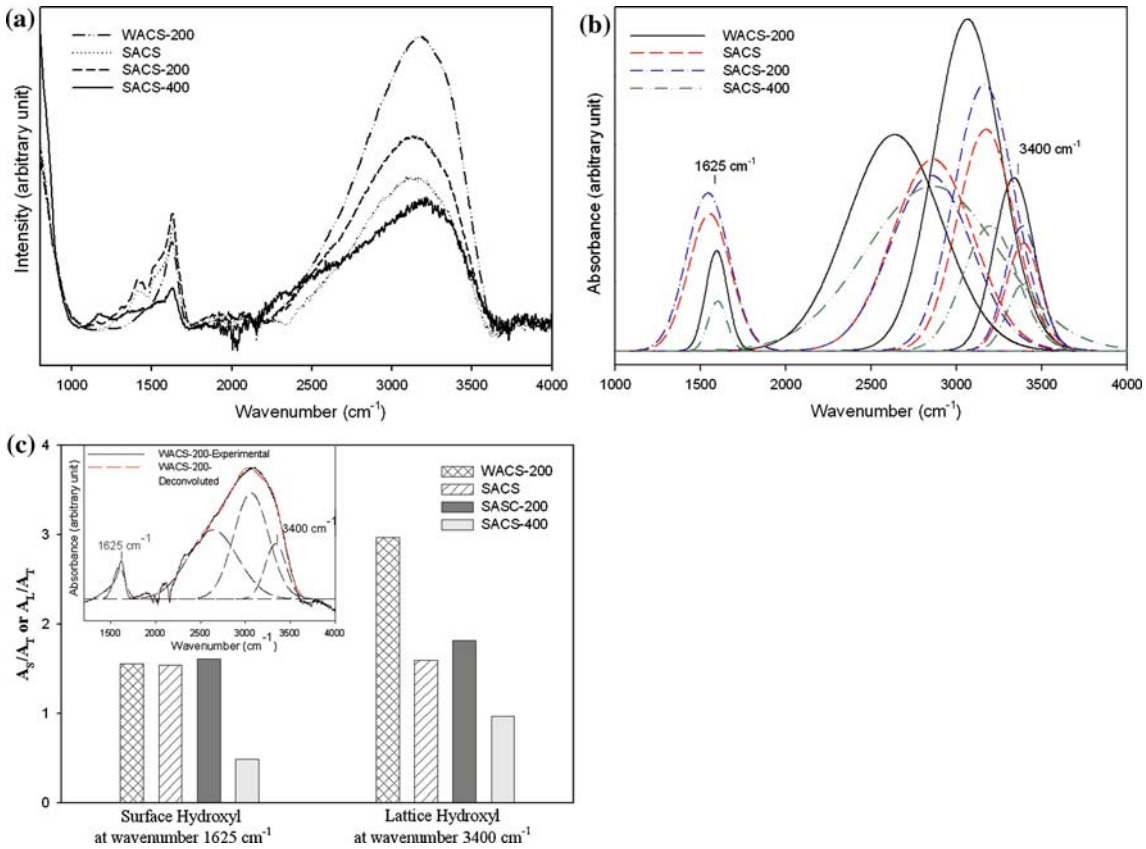

Fig. 5 (**a**) FT-IR spectra using ATR of the prepared titania samples; (**b**) deconvolution of the FT-IR spectra; (**c**) ratio (A_S/A_T) of absorbance by FI-IR spectra of surface hydroxyls (A_S) or lattice hydroxyls (A_L) to the reference peak (A_T) at wavenumber 900 cm^{-1}; and inset of (**c**) shows FT-IR spectra using ATR of the prepared titania samples

relatively, has significantly larger lattice hydroxyls peaks than SACS, SACS-200, and SACS-400, since the solvothermal treatment extracted the lattice hydroxyls from the titania particles. The surface hydroxyls of SACS and SACS-200 are similar to WACS-200. However, SACS-400 shows significantly fewer surface hydroxyls than samples calcined at lower temperatures. The surface hydroxyl can be removed by heat treatment at temperatures above 200 °C.

Figure 6a, b depict the photocatalytic activities of polymorphic titania samples compared to P25 samples, determined by the methyl orange degradation under UV exposure. As a time comparison to degrade methyl orange, 80% of total methyl orange degraded is arbitrarily chosen. As shown in Fig. 6a, the degradation by SACS and SACS-200 samples is approximately 60% faster than WACS and WACS-200 even though SACS samples have a lower surface area than WACS. Compared to the previous research [16] on SACS samples prepared in sec-butanol, the degradation by SACS prepared in NMP solvent samples is two times faster than in sec-butanol. The research on SACS in sec-butanol found that with greater lattice hydroxyl content in polymorphic titania, the lower the photocatalytic activity. Therefore, the superior photocatalytic activity of SACS samples is due to not only fewer lattice hydroxyls but also nitrogen present in SACS samples. FT-IR data supported that fewer lattice hydroxyl are found in SACS samples than in WACS samples. The lattice hydroxyl may produce Ti–OH bonds as defects in the titania lattice structures [45]. It has been reported in the literature [46–50] that bulk defects decrease the photocatalytic activity since these defects produce sites for the recombination of electrons and holes. In order to increase the photocatalytic activity of TiO_2, reducing OH defects by extracting $^{-}$OH from the lattice is necessary. Polymorphic TiO_2 (SACS, SACS-200, WACS, and WACS-200), with three times larger surface area than P25, yielded a higher photocatalytic activity than P25, as expected. The effect of calcination temperature of SACS samples on MO degradation activity is shown in Fig. 6b. The photocatalytic activity, under UV exposure, of SACS samples, calcined at various temperatures, increased in the following order: SACS ≅ SACS-200 ≅ SACS-250 > SACS-300 >> SACS-350 > SACS-400 ≅ SACS-500. The orange color of MO did not completely degrade within 120 min by UV irradiating SACS-400 and SACS-500. The increase of treatment temperature up to 400 and 500 °C not only reduces the surface area, but also changes the phase

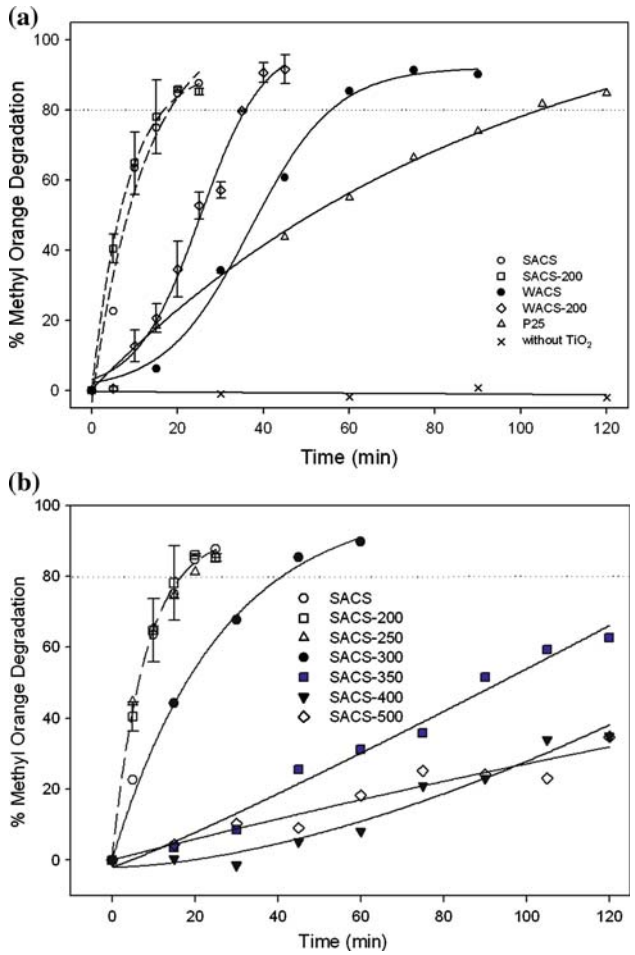

Fig. 6 Methyl orange degradation under UV light of (**a**) uncalcined and calcined WACS and SACS samples compared to commercial P25 and (**b**) SACS samples calcined at vary temperature

composition, increasing rutile while sacrificing brookite and anatase. The lower surface area, elimination of nitrogen, and higher rutile content [9, 23] caused a reduction of photocatalytic activities. According to our CHNS analysis results, the more nitrogen presents in TiO_2, the higher the photocatalytic activity under both UV and VL exposure. This is consistent with the results of Aita et al. and Irie et al. [19, 20]. Nitrogen doped titania in SACS and SACS-200 showed a significant band gap narrowing, as found from UV/Vis spectra, which resulted in an increase in VL photocatalytic activity. The results may well agree with the observation made by Li et al. for their anatase titania with MO decolorization [51]. Preliminary results of MO degradation under VL irradiation in Fig. 7 confirmed that SACS-200 has a much higher VL photocatalytic activity than WACS-200 and Degussa P25. VL activated SACS-200 completely degraded MO after 1 h. WACS-200 and P25 did not show the MO degradation after VL irradiation for 16 h. The time

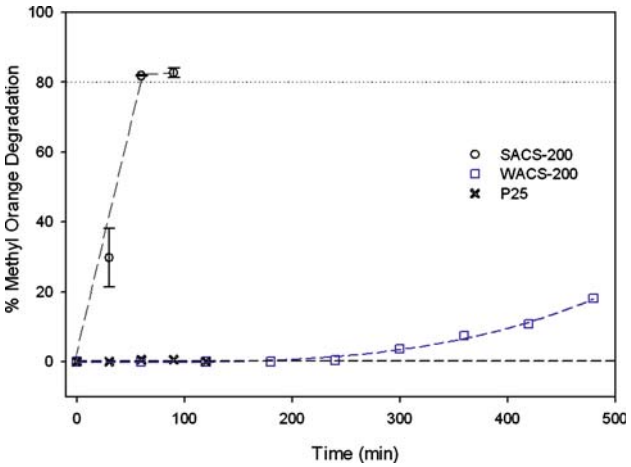

Fig. 7 Methyl orange degradation under VL irradiation of SACS-200, WACS-200 and P25

to decolorize MO is relative since the visible light source is a low intensity custom-designed lamp.

4 Conclusions

Solvothermal post-treatment technique, using NMP as the solvent, is a useful method to extract lattice hydroxyls and to decorate nitrogen on the titania surface or in the structure as shown in the comparison between WACS and SACS. The greater the number of lattice hydroxyls in polymorphic titania, the lower the photocatalytic activity. The more nitrogen presents in SACS samples, the higher the photocatalytic activity. SACS-200 showed the best photocatalytic activity under both UV and VL irradiation among prepared titania samples and P25. Therefore, in this study, the optimum calcination temperature for SACS samples is 200 °C for 2 h. Moreover, other calcination variables such as time and calcination atmosphere, which can potentially influence the phase composition and structure and thus the photocatalytic activity, are being investigated.

Acknowledgment This research was supported by the state of South Carolina and the Petroleum Research Fund of American Chemical Society. The authors gratefully acknowledge Kimberly A. Ivey, School of Materials Science and Engineering, Clemson University for all FT-IR data.

References

1. Fujishim A, Honda K (1972) Nature 238:37
2. Hoffmann MR, Martin ST, Choi WY, Bahnemann DW (1995) Chem Rev 95:69
3. Linsebigler AL, Lu GQ, Yates JT (1995) Chem Rev 95:735
4. Matthews RW (1988) J Catal 111:264
5. Pelizzetti E (1995) Sol Energ Mat Sol C 38:453

6. Tryk DA, Fujishima A, Honda K (2000) Electrochim Acta 45:2363
7. Lee BI, Wang XY, Bhave R, Hu M (2006) Mater Lett 60:1179
8. Bhave RC, Lee BI (2007) Mat Sci Eng A Struct 467:146
9. Nolph CA, Sievers DE, Kaewgun S, Kucera CJ, McKinney DH, Rientjes JP, White JL, Bhave R, Lee BI (2007) Catal Lett 117:102
10. Degussa (2005) In: Degussa technical information, vol 1243
11. Sato T, Aita Y, Komatsu M, Yin S (2006) J Mater Sci 41:1433
12. Yin S, Fujishiro Y, Wu JH, Aki M, Sato T (2003) J Mater Process Tech 137:45
13. Yin S, Inoue Y, Uchida S, Fujishiro Y, Sato T (1998) J Mater Res 13:844
14. Yin S, Sato T (2000) Ind Eng Chem Res 39:4526
15. Yin S, Aita Y, Komatsu M, Wang JS, Tang Q, Sato T (2005) J Mater Chem 15:674
16. Kaewgun S, Nolph CA, Lee BI, Wang L-Q (2007) Appl Catal A: Gen J (Submitted)
17. Kota R, Lee BI (2007) J Mater Sci: Mater Electron 18:1221
18. Qi L, Lee BI, Badheka P, Wang LQ, Gilmour P, Samuels WD, Exarhos GJ (2005) Mater Lett 59:2794
19. Aita Y, Komatsu M, Yin S, Sato T (2004) J Solid State Chem 177:3235
20. Irie H, Watanabe Y, Hashimoto K (2003) J Phys Chem B 107: 5483
21. Zhang HZ, Banfield JF (2000) J Phys Chem B 104:3481
22. JCPDS #29-1276
23. Li JG, Ishigaki T, Sun XD (2007) J Phys Chem C 111:4969
24. Birks LS, Friedman H (1946) J Appl Phys 17:687
25. Lee BI (1999) J Electroceram 3:53
26. Lu SW, Lee BI, Mann LA (2000) Mater Lett 43:102
27. Lu SW, Lee BI, Mann LA (2000) Mater Res Bull 35:1303
28. JCPDS #29-1272
29. JCPDS #29-1360
30. Asahi R, Morikawa T, Ohwaki T, Aoki K, Taga Y (2001) Science 293:269
31. Chi B, Zhao L, Jin T (2007) J Phys Chem C 111:6189
32. Joung SK, Amemiya T, Murabayashi M, Itoh K (2006) Appl Catal A Gen 312:20
33. Kang IC, Zhang QW, Kano J, Yin S, Sato T, Saito F (2007) J Photochem Photobiol A 189:232
34. Matsumoto T, Iyi N, Kaneko Y, Kitamura K, Ishihara S, Takasu Y, Murakami Y (2007) Catal Today 120:226
35. Nakamura R, Tanaka T, Nakato Y (2004) J Phys Chem B 108:10617
36. Sathish M, Viswanathan B, Viswanath RP, Gopinath CS (2005) Chem Mater 17:6349
37. Venkatachalam N, Vinu A, Anandan S, Arabindoo B, Murugesan V (2006) J Nanosci Nanotechnol 6:2499
38. Yin S, Aita Y, Komatsu M, Sato T (2006) J Eur Ceram Soc 26:2735
39. Burda C, Lou YB, Chen XB, Samia ACS, Stout J, Gole JL (2003) Nano Lett 3:1049
40. Chen XB, Burda C (2004) J Phys Chem B 108:15446
41. Moulder JF, Stickle WF, Sobol PE, Bomben KD (1995) In: Chastain J, King RC (eds) Handbook of X-ray photoelectron spectroscopy. Physical Electronics, Inc
42. Munoz MA, Carmona C, Balon M (2007) Chem Phys 335:37
43. Suda Y, Morimoto T (1987) Langmuir 3:786
44. Zheng YQ, Erwei S, Cui SX, Li WJ, Hu XF (2000) J Mater Sci Lett 19:1445
45. Hayashi H, Torii K (2002) J Mater Chem 12:3671
46. Howe RF, Gratzel M (1985) J Phys Chem-US 89:4495
47. Howe RF, Gratzel M (1987) J Phys Chem-US 91:3906
48. Kongsuebchart W, Praserthdam P, Panpranot J, Sirisuk A, Supphasrirongjaroen P, Satayaprasert C (2006) J Cryst Growth 297:234
49. Nakaoka Y, Nosaka Y (1997) J Photochem Photobiol A 110:299
50. Ohtani B, Ogawa Y, Nishimoto S (1997) J Phys Chem B 101:3746
51. Li M, Hong Z, Fang Y, Huang F (2007) Mater Res Bull (in press)